Materials Today Bio 16 (2022) 100346

Contents lists available at ScienceDirect

Materials Today Bio

journal homepage: www.journals.elsevier.com/materials-today-bio

Designer tetrahedral DNA framework-based microfluidic technology for multivalent capture and release of circulating tumor cells

Chenguang Wang [a,b,c,d,1], Yi Xu [c,1], Shuainan Li [c,d], Yi Zhou [e], Qiuling Qian [c,d], Yifan Liu [f], Xianqiang Mi [a,b,c,d,g,h,*]

[a] State Key Laboratory of Functional Material for Informatics, Shanghai Institute of Microsystem and Information Technology, Chinese Academy of Sciences, Shanghai, 200050, China
[b] CAS Center for Excellence in Superconducting Electronics (CENSE), Shanghai, 200050, China
[c] Shanghai Advanced Research Institute, Chinese Academy of Sciences, Shanghai, 201210, China
[d] University of Chinese Academy of Sciences, Beijing, 100049, China
[e] College of Basic Medicine, Chengdu University of Traditional Chinese Medicine, Chengdu, 611137, China
[f] Division of Chemistry and Physical Biology, School of Physical Science and Technology, ShanghaiTech University, Shanghai, 201210, China
[g] Key Laboratory of Systems Biology, Hangzhou Institute for Advanced Study, University of Chinese Academy of Sciences, Chinese Academy of Sciences, Hangzhou, 310024, China
[h] Key Laboratory of Systems Health Science of Zhejiang Province, Hangzhou Institute for Advanced Study, University of Chinese Academy of Sciences, Hangzhou, 310024, China

ARTICLE INFO

Keywords:
Tetrahedral DNA framework
Aptamer
Hybridization chain reaction
Circulating tumor cell
Microfluidic chip

ABSTRACT

Circulating tumor cells (CTCs) have been recognized as a general biomarker for the early detection, diagnosis and therapy monitoring of cancer. Due to their extreme rarity in peripheral blood, the isolation and analysis of CTCs with high efficiency, high purity and high viability remains a tremendous technological challenge. Herein, we combined tetrahedral DNA framework (TDFs), herringbone channel (HB) chip, together with aptamer-triggered hybridization chain reaction (apt-HCR) to develop an efficient microfluidic system (T-μFS) for capture and release of simulated CTCs. The capture efficiency of MCF-7 cells was from 83.3% to 94.2% when the cell numbers ranged from 10 to 10^3 using our T-μFS in the whole blood. The release efficiency of the MCF-7 cells was 96.2% and the MCF-7 cell viability after release was 94.6% using our T-μFS in PBS buffer. Reculture and RT-qPCR studies showed that there was almost no damage by the capture and release treatment for the MCF-7 cells viability. These results revealed that our T-μFS could be developed as an integrated and automatic technical platform with great performance for multivalent capture and release of CTCs and have a wide application prospect for tumor liquid biopsy.

1. Introduction

Circulating tumor cells (CTCs) shed from primary or metastatic lesions, carrying significant information of cancer progression and metastasis [1,2]. CTCs have been recognized as the general biomarker for the early detection, diagnosis and therapy monitoring of cancer which have been regarded as "liquid biopsies" [3,4]. There has been a tremendous technological challenge in enriching and characterizing CTCs with high efficiency and purity because CTCs are extremely rare (only several CTCs in a billion blood cells) [5]. In recent years, numerous platforms have been disclosed to capture and analyze CTCs [6,7]. Biological affinity strategies based on the specific binding between bioprobes and target CTCs have been most widely used for capturing CTCs [8].

Aptamers are oligonucleotide sequences of DNA or RNA which show great promise as capture ligands including low cost, high storage stability, small size and reproducible quality [9]. Aptamer-based bio-affinity methods by combining aptamers with nanoparticles could enhance the capture performance of CTCs [10,11]. However, these methods still could not meet the needs of high efficiency and purity for capturing CTCs [12]. Hybridization chain reaction (HCR) is a novel toehold-mediated

* Corresponding author. State Key Laboratory of Functional Material for Informatics, Shanghai Institute of Microsystem and Information Technology, Chinese Academy of Sciences, Shanghai, 200050, China.
E-mail address: mixq@mail.sim.ac.cn (X. Mi).
[1] Equal contributing authors.

https://doi.org/10.1016/j.mtbio.2022.100346
Received 7 May 2022; Received in revised form 26 June 2022; Accepted 27 June 2022
Available online 2 July 2022

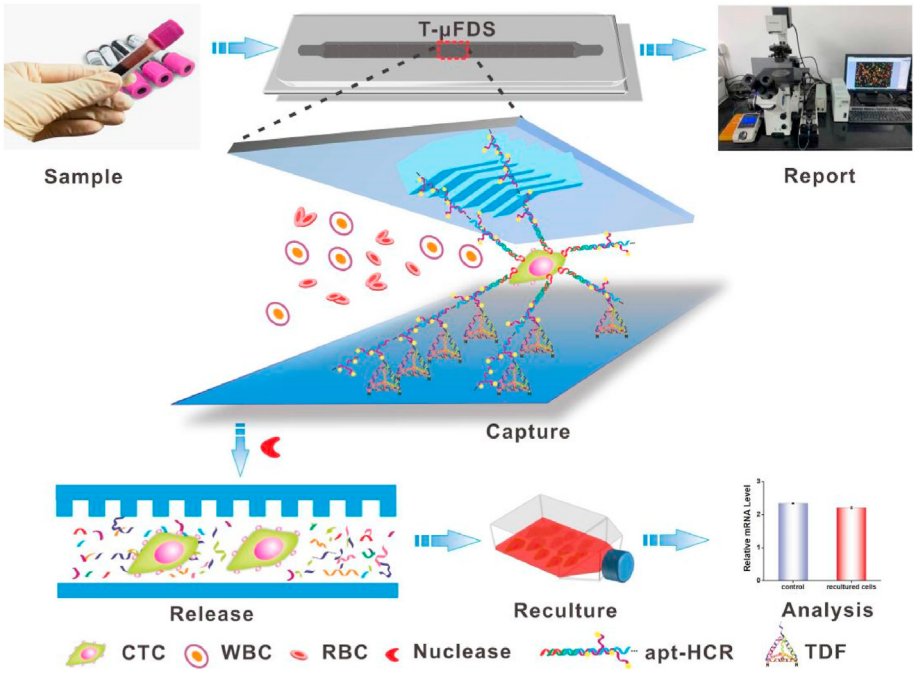

Scheme 1. Working principle of the T-μFS. When CTCs were recognized and bound to apt-HCR, the apt-HCR/CTCs complex was hybridized with the TDFs fixed on the glass surface, while white blood cells (WBCs) and red blood cells (RBCs) could not be recognized and bound. The upper PDMS cover with HB structure as micro-mixer could increase the contact frequency between TDFs and CTCs. Upon nuclease treatment, TDF and apt-HCR could be specifically cleaved, releasing CTCs for downstream analysis.

strategy which could achieve signal amplification with fluoresce output molecules [13,14]. HCR triggered by aptamers could form a long-chain complex which is the promising way to achieve sensitive capture of CTCs. For example, Yuan et al. developed a split aptamer-based dual HCR for highly sensitive and specific capture of rare tumor cells [15].

The emerging microfluidic technologies can integrate the entire laboratory into a single chip, providing a potential platform for capturing CTCs with advantages such as high throughput and automatic operation [16]. The typical microfluidic chip for CTCs' capture consists of upper cover and lower substrate. The upper layer is generally used as micro-mixer with micro/nano-structure to realize passive mixing. One hallmark micro-mixer, first introduced by Stroock et al. was the staggered grooved-herringbone (HB) structure which could stretch and fold the liquid flows in the cross-section, yielding chaotic flows that are essential for generating efficient mixing [17,18]. The lower layer is generally used as solid substrate to immobilize capture probes which is often modified by nanostructures such as nanowires [19], nanoparticles [20], nanosheets [21] which could provide more surface area and higher loading capacity [22].

Currently, most analysis of captured CTCs is accomplished by directly lysing cells on the surface of the device for downstream enzymatic reactions to measure DNA or proteins [23]. However, the value of the rare cells captured is much more than that. The downstream analysis of CTCs has received increasing attention and has become the focus of CTC research. One of the important prerequisites of CTC downstream analysis is to release the captured CTCs from affinity-adhered substrates while keeping cells viable, but due to the vulnerability of CTCs, many studies cannot meet the requirement of efficient release of CTCs while ensuring high capture efficiency [10,24,25]. The existing CTCs release technologies such as laser microdissection [26], magnetic fields [27], thermal denaturation [28], shear stress-mediated elution [29], chemical reaction [30] et al. were limited by damaging the cell membrane and affecting cells' viability. Enzyme digestion is one of the most common methods for CTCs' release [31]. Nuclease has been used for CTC release without destroying the surface proteins of cell membrane, and had little effect on cells' viability [32,33]. It was reported that high-speed rinsing together with enzyme digestion could improve the release efficiency of the captured CTCs in a shorter time [25].

The three-dimensional tetrahedral DNA framework (TDF) is a kind of self-assembled DNA nanostructure with excellent controllability and high precise orientations [34,35]. TDFs based capture probes have been widely used for DNA, microRNA, protein and CTCs detection [36–39]. TDFs can be easily fixed on the solid substrates by binding covalently for their mechanical rigidity and structural stability [40]. Moreover, compared with other traditional nanostructures, TDFs are nucleotide based nanostructures which could easily be degraded by nuclease to obtain nondisrupted CTCs [41].

Herein, for the first time we combined aptamer-triggered hybridization chain reaction (apt-HCR), herringbone channel (HB) chip, together with amino-modified tetrahedral DNA framework (TDFs) to construct a microfluidic system (T-μFS) (Scheme 1). The TDFs in our design could be used as scaffolds to be fixed on the glass substrate of the HB-chip and hybridized with the multiple branched arms of apt-HCR products to achieve multivalent binding of CTCs. As the TDFs were DNA nanostructures, they could be specifically removed through benzonase nuclease, which promoted CTCs to release without damaging the cells. With the help of herringbone channels, more effective contact between CTCs and captured probes was achieved, resulting higher capture and release efficiency for downstream analysis.

2. Materials and methods

2.1. Materials and reagents

All DNA sequences (Table S1) were ordered from Shanghai Sangon Bioengineering Technology and Services. DMEM medium (high glucose), Pen Strep, FBS (Fetal Bovine Serum, Qualified), 0.25% Trypsin-EDTA (1×) were purchased from gibco. CellTracker™ Green CMFDA, CellTracker™ Blue CMAC, calcein (AM), Ethidium homodimer-1 (EthD-1) were purchased from invitrogen. Red blood cell lysing buffer was purchased from HaoYang Biological Manufacture Co., TianJin, China. Benzioase nuclease was purchased from sigma-aldrich. Healthy human blood samples with the anticoagulant ethylenediaminetetraacetic acid (EDTA) were donated by volunteers. The DOWSIL™ 184 polydimethylsiloxane (PDMS) pre-polymer and curing agent were purchased from Dow Corning. Aldehyde-functionalized glass slide was purchased from CapitalBio Corp, BeiJing, China. 1 mL syringe and PTFE catheter were purchased from Wenhao, Suzhou, Co., Ltd. One Step RT-qPCR Kit and total RNA

Extractor (Trizol) were purchased from Sangon Biotech, Shanghai, Co., Ltd. Other reagents (analytical grade) involved in the experiment were purchased from Sangon Biotech, Shanghai, Co., Ltd.

2.2. Instruments

Micro syringe pump was purchased from Longer pump, Baoding, China. NanoDrop Lite spectrophotometer was purchased from Thermo Fisher Scientific, USA. O_2 plasma cleaner (YZD08-2C) was purchased from SAOT (Beijing) Tech Co., Ltd. Fluorescent Microscope used was Olympus IX71 (Olympus, Tokyo, Japan). Flow cytometry used was BD LSRFortessa™ Cell Analyzer (BD Biosence, USA).

2.3. Cell culture

Human breast cancer cell line (MCF-7) and human cervical cancer cell line (Hela) were cultured with DMEM comprising FBS (10%) and Pen Strep (1%) and were incubated in humid atmosphere at 37 °C with 5% CO_2.

2.4. Synthesis and characterization of TDFs and HCR structures

TDFs were formed based on modified literature protocols [42]. Briefly, the tetra-A strand fragment (80-base) and the three amino-modified single DNA strand fragments (tetra-B, tetra-C, and tetra-D, 55-base) (Table S1) were dissolved in TE buffer (10 mM Tris, 1 mM EDTA, pH8.0) to final concentration of 100 μM separately. 1 μL each kind of single DNA strand fragment was mixed with 96 μL TM buffer (20 mM Tris, pH8.0). The resulting mixture was heated by use of a T100™ PCR thermal cycler (95 °C for 10min and then cooled to 4 °C for 30s). TDFs were further identified by native polyacrylamide gel electrophoresis (PAGE). 8% polyacrylamide gel (6 mL) was prepared with 30% acryl/bis solution (1.6 mL), $MgCl_2$ (0.75 mL), 5 × TBE (1.2 mL) and Milli-Q water (2.45 mL). Then 60 μL of ammonium persulfate (APS) and 6 μL of 1,2-di-(dimethylamino)ethane (TEMED) were added into the gel and mixed gently for further use. All of the DNA samples were run at 100 V for 120 min and stained with GelRed for 15 min before visualizing under UV light. The triple-strand DNA combinations, double-strand DNA combinations and single-strand DNA fragments were also synthesized and identified in the same way.

HCR structures were formed as the method reported [43]. Briefly, initiator strand (10 μM), H1 strand (10 μM) and H2 strand (10 μM) were heated separately by use of a T100™ PCR thermal cycler (95 °C for 2min and then cooled to room temperature for 1 h). After that, Initiator with different final concentration (0.1 μM, 0.2 μM, 0.5 μM and 1 μM) was mixed with H1 and H2 to final concentration of 1 μM respectively in TM buffer, then they were incubated at 37 °C for 2 h to form HCR structures. HCR structures were further identified by agarose gels electrophoresis. The 1% agarose gel was prepared with 1 × TAE buffer (40 mM Tris−acetate and 1 mM EDTA, pH 8.0). After the gel was heated in a microwave oven to dissolve completely, added 1/10,000 ethidium bromide solution. The samples were run at 150 V for 60 min and visualized under UV light. To synthesize apt-HCR, aptamer and initiator strands with equal proportions were mixed in TM buffer. Then, aptamer and initiator mixture (1 μM), H1(10 μM) and H2(10 μM) were heated separately. After that, 20 μL PCR product of aptamer and initiator mixture (apt/I) solution was added to 180 μL PCR product of H1 and H2 (1:1) solution with approximate final concentrations of 0.1, 1 and 1 μM for apt/I, H1 and H2, respectively. Then apt/I, H1 and H2 mixture solution was incubated at 37 °C for 2 h to form apt-HCR structure.

2.5. Affinity binding analysis of Apt-HCR toward target cells

To prove that the apt-HCR structure could recognize target cells and amplify the labeled fluorescence signal, 10^5 MCF-7 cells or 10^5 Hela cells were incubated with apt-HCR products with Cy3 fluorophores labeled at the 5′ end of the H1 and H2 respectively in 200 μL TM buffer for 30 min on ice to obtain apt-HCR/cells complex. After incubation, the apt-HCR/cells complex was washed with PBS (10 mM phosphate buffer, 0.14 M NaCl, 2.7 mM KCl, pH 7.4) for at least three times to wash away unbinding apt-HCR, then was resuspended in the PBS and counted by the flow cytometer. Other experiments' protocol using Cy3-labeled single SYL3c aptamer (apt), Cy3-labeled random sequence strand (lib) and random sequence strand triggered HCR (lib-HCR, Cy3-labeled H1 and H2 respectively) toward MCF-7 cells or 10^5 Hela cells was the same as above.

To calculate the equilibrium dissociation constant value (K_d), the apt-HCR product was formed as described in Section 2.4, the final concentrations of apt/I were 0 nM,1 nM, 2 nM, 3 nM, 5 nM, 10 nM, 20 nM, 50 nM, 100 nM, and 150 nM respectively, while the final concentrations of H1 and H2 were 1 μM in apt/I, H1 and H2 mixture solution. Each apt-HCR structure was incubated with 10^5 MCF-7 cells, washed with PBS and resuspended in the PBS as above, then counted by the flow cytometry. The dissociation constant (K_d) was obtained by fitting the dependence of fluorescence intensity with the final concentration of apt/I by the equation $Y = B_{max}X/(K_d + X)$ using SigmaPlot software (Jandel, San Rafael, CA, USA), where Y is the fluorescence intensity and X is the concentration of apt/I.

Fluorescence microscope was also used to evaluate the bio-affinity binding capabilities of apt-HCR toward MCF-7 cells. 10^5 MCF-7 cells were incubated with apt-HCR, washed with PBS, resuspended in the PBS as above, then observed under the microscope.

To prove the feasibility of combining apt-HCR with TDFs, TDFs and apt-HCR were hybridized in TM buffer with each final concentration of TDF and H1, H2 was 1 μM. The products were further identified by 1% agarose gels.

2.6. Fabrication of the microfluidic chip

The design of the herringbone microfluidic chip was inspired by several works in the literature [17,18]. The detailed dimensions of PDMS layer with herringbone structure (HB channel) was shown in Fig. S3. The HB channel was staggered periodically, with each mixing cycle defined by two sequential regions of ten chevrons shifted asymmetrically, angle between the herringbones and the axis of the channel (θ) was 45°. The dimension of the HB channel was 50 mm × 2 mm × 50 μm (L × W × H). The PDMS cover was prepared by mixing DOWSILTM 184 pre-polymer solution and curing agent (10:1). Inlet and outlet wells were created at the channel ends by punching holes in the PDMS layer. Aldehyde-functionalized glass slide was protected by self-made cap and sealed with the PDMS layer by O_2 plasma cleaner for 15 s with the power 200 W. To fix TDFs on the glass substrate, 10 μL TDFs solution (1μM) was first pumped into the chip and incubated overnight at room temperature in a humidity chamber. The chip was rinsed with 100 μL PBS to remove the unbinding TDFs.

2.7. Cell capture assay in the T-μFS

The T-μFS mainly included the PTFE catheter, syringe pump, the microfluidic chips and fluorescence microscope.

To prove the capture effectiveness of HB-chip and optimize the flow rate in the T-μFS, we designed two experiments using TDF-modified HB-chip and flat-chip separately. For either of the experiments, 10^5 MCF-7 cells were stained with CellTracker™ Green CMFDA. The labeled MCF-7 cells were incubated with apt-HCR in 200 μL TM buffer for 1 h on ice, washed with PBS at least three times to wash away unbinding apt-HCR, then apt-HCR/MCF-7 complex was spiked in 200 μL PBS buffer. For TDF-modified HB-chip or flat-chip experiments at different flow rate (2 μL/min, 5 μL/min, 10 μL/min, 15 μL/min, 20 μL/min), apt-HCR/MCF-7 cells (10^5) complex solution in 200 μL PBS buffer was pumped into the T-μFS. After the apt-HCR/MCF-7 complex was captured, 100 μL PBS was injected to remove uncaptured cells. Subsequently, the captured MCF-7 cells were observed and counted using a fluorescence microscope. The

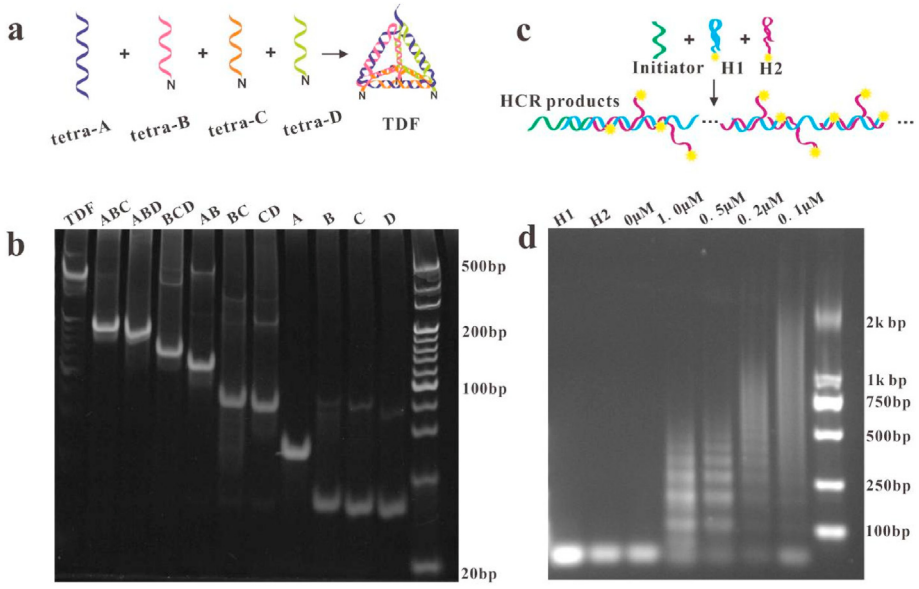

Fig. 1. Characterization of TDFs and HCR structures. (a) Schematic for synthesis of TDFs. (b) Polyacrylamide gel electrophoresis image of different DNA strands. From left to right: TDF, triple-strand DNA combinations (ABC, ABD, BCD), double-strand DNA combinations (AB, BC, CD), single-strand DNA fragments (A, B, C, D), 500-bp DNA ladder marker. (c) Schematic for synthesis of HCR. (d) Agarose gel electrophoresis image of HCR products by initiator with different concentrations. From left to right: lane 1 and 2, 1.0 μM H1 and 1.0 μM H2; lane3-7, initiators with five different concentrations (0.0, 1.0, 0.5, 0.2, and 0.1 μM) in 1 μM mixture of H1 and H2; lane8, 2000-bp DNA ladder marker.

capture efficiency was defined as the number ratio of target cells captured to target cells initially seeded.

In the following experiments, the methods of staining MCF-7 cells, formation of aptamer/MCF-7 cells complex, removing uncaptured cells, cell observation and count were the same as described above.

To prove the capture effectiveness of TDFs connected apt-HCR (T-A-HCR) for CTCs in T-μFS, we designed three experiments including single-strand DNA connected aptamer (E-apt), TDF connected aptamer (TDF-apt) and T-A-HCR to compare their capture efficiency for MCF-7 cells (Table S1). 10^5 MCF-7 cells were stained and capture probes (aptamer or apt-HCR)/MCF-7 cells complex was spiked in 200 μL PBS buffer. For either of the E-apt or TDF-apt experiments, the aptamer/MCF-7 cells complex in PBS buffer was pumped into the single-strand DNA-modified HB-chip or TDF-modified HB-chip respectively. For apt-HCR experiments, the apt-HCR/MCF-7 cells complex in PBS buffer was pumped into the TDF-modified HB-chip. After the MCF-7 cells were captured, uncaptured cells were removed, then the captured cell was observed and counted.

To explore the capture efficiency of the T-μFS for MCF-7 cells with different concentrations, 10^5 MCF-7 cells was resuspended in 200 μl PBS buffer, stored on ice and further diluted to the desired concentrations (10 to10^5). The MCF-7 cells were stained and the apt-HCR/MCF-7 cells complex was formed. When used for cell capture, the apt-HCR/MCF-7 cells complex in PBS buffer was pumped into the T-μFS. After the target cells were captured, uncaptured cells were removed, then the captured cell was observed and counted.

To explore the capture purity of the T-μFS, MCF-7 (10^5) and Hela (10^5, stained with Blue CMAC) cells were incubated with apt-HCR to obtain apt-HCR/MCF-7/Hela cells mixture complex. The complex was resuspended in 200 μL PBS, stored on ice and further diluted to the desired numbers (10^3, 10^4, 10^5). When used for cell capture, the cells' mixture complex in 200 μL PBS buffer was pumped into the T-μFS. After the target cells were captured, uncaptured cells were removed, then the captured cell was observed and counted. The purity was defined as the number ratio of the MCF-7 cells captured to total cells.

2.8. Study on the clinical utility of the T-μFS

To study the clinical utility of the T-μFS by mimic blood samples, the human whole blood was obtained from volunteers. 100 mL of whole blood was added to 100 mL of PBS buffer, mixed well and placed at 4 °C for later use. The lysed blood was obtained by adding red blood cell lysing buffer (1 mL) to the whole blood (200 μL), mixed by gently pipetting and lysed for 2 min, then centrifuged at 300 g for 10 min and discarded the red supernatant. After the red blood cells were completely lysed, washed and resuspended with PBS buffer. The lysed blood placed at 4 °C for later use. 10^5 stained MCF-7 cells were spiked in 200 μL of lysed blood or whole blood and incubated with apt-HCR for 1 h, then washed with PBS for at least three times. The apt-HCR/MCF-7 cells complex was diluted to different numbers (10-10^3) and resuspended in 200 μl lysed blood or whole blood. When used for cell capture, apt-HCR/MCF-7 cells complex in lysed blood or whole blood was pumped into the T-μFS. After the target cells were captured, uncaptured cells were removed, then the captured cell was observed and counted.

2.9. Release and reculture assay

The apt-HCR/MCF-7 (10^3) complex was obtained in 200 μL PBS buffer and pumped into the T-μFS. After MCF-7 cells were captured at optimized conditions as described in Section 2.7, benzonase nuclease (25 units/mL) in 10 μl PBS buffer was introduced into the T-μFS.

To study the optimal enzyme digestion incubation time for releasement of the captured MCF-7 cells, the apt-HCR/MCF-7 complex was incubated at 37 °C with benzioase nuclease for 5, 10, 15, 20, and 30 min in the T-μFS, then rinsed at the flow rate of 5 μL/min. To study the optimal rinsing flow rate for releasement of the captured MCF-7 cells, the T-μFS with captured MCF-7 cells was rinsed at the flow rate of 5 μL/min, 10 μL/min, 15 μL/min, 20 μL/min and 30 μL/min respectively after optimal enzyme digestion time. The released MCF-7 cells were observed and counted using the fluorescence microscope. The release efficiency is defined as the number ratio of the released cells to captured cells.

To study the MCF-7 cells' viability, MCF-7 cells were captured and released at the optimal nuclease incubation time and rinsing flow rate. The MCF-7 cells being captured and after releasement were stained with Calcein-AM/EthD-1 mixture in PBS buffer (with 2 μM Calcein-AM and EthD-1 respectively) for 10 min, then observed by fluorescent microscope. Viable and dead cells were stained by Calcein-AM(green) and EthD-1(red) respectively. The cell viability is defined as the number ratio of viable cells (green) to total cells (green + red).

To realize cell reculture and morphological observation, MCF-7 cells were captured and released at the optimal nuclease incubation time and rinsing flow rate. The released MCF-7 cells were collected in a new cell culture dish and put into the incubator for continuous morphological observation. After the dish was fully covered with recultured MCF-7 cells,

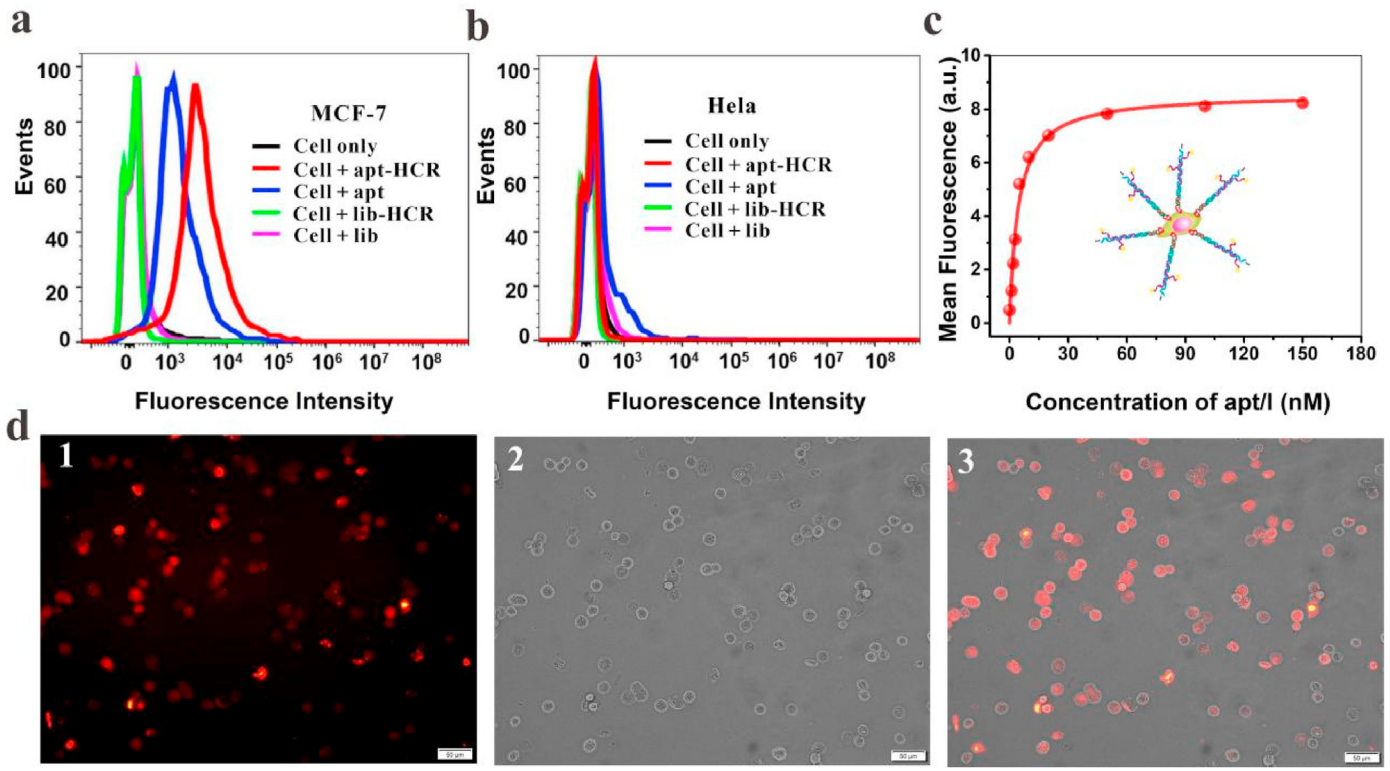

Fig. 2. Flow cytometry and fluorescence microscope analysis for affinity binding behavior between apt-HCR and target cells. (a) For MCF-7 cell line experiment, MCF-7 cells selectively bond with apt-HCR and apt probes, while not bond with lib and lib-HCR probes. (b) For the control Hela cell lines experiment, Hela cells did not bind with apt-HCR, apt, lib and lib-HCR probes. (c) Flow cytometry analysis to determine the dependence of the fluorescence signal of the MCF-7 cells to the concentrations of apt/I. (d) Fluorescence microscope image of (1) Cy3 modified apt-HCR (2) MCF-7 cells (3) merged picture (Scale bar = 50 μm).

the cells were digested with trypsin for molecular analysis. The mRNA expression of CK19 and EGFR was analyzed by quantitative real-time RT-PCR (qPCR). Total RNA was extracted with Total RNA Extractor (Trizol). The concentrations of all RNA samples were quantified using a NanoDrop Lite spectrophotometer. qPCR was performed using One Step RT-qPCR Kit. The sequences of primers for qPCR were shown in Table S1.

3. Results and discussion

3.1. Synthesis and characterization of TDFs and HCR structures

The pyramidal TDF we designed contained a pendant probe at the top vertices which could bind with apt/HCR structure for CTCs capture and three amine groups at the bottom vertices which could be fixed on the solid substrate (Fig. 1a). TDFs, double-strand DNA fragment combinations (AB, BC, CD) and triple-strand DNA fragment combinations (ABC, ABD, BCD) were synthesized and confirmed through PAGE. We also characterized the morphology of TDFs on the mica surface by using atomic force microscopy (AFM), which indicated that the structure of TDFs was uniform and no aggregates appeared on the surface (Fig. S1). The size of TDF contained 17 base pairs on each edge, and the corresponding theoretically calculated edge length was 5.8 nm. As shown in Fig. 1b, The TDFs shifted much slower than the triple-strand DNA fragment combination, double-strand DNA fragment combination and single-strand DNA fragment which confirmed that the TDF was successfully formed as it had larger size and weight.

The hairpin polymerization was triggered by an initiator (I) and two fluorophore-labeled hairpins (H1 and H2) as fuel chains. Based on rational design, the initiator was partially complementary to the aptamer sequences. Cy3 fluorophores were modified at 5′end of H1 and H2 hairpins respectively, and the extension part in long stem region of H2 hairpin structure could be used as multi-branched arms for hybridized with TDFs (Fig. 1c). By thermodynamic calculation through the DINA-Melt Web Server, both the modified H1 and H2 hairpin structure with a short loop region and a long stem region are stable enough to keep the "hairpins" without the initiator (Table S2). The stable state was disturbed by the initiator and the fuel chains when introducing the initiator, HCR reaction was triggered by alternating addition of H1 and H2, then the HCR products could be achieved (Fig. 1c). As shown in Fig. 1d, initiators with four different concentrations (0.1 μM, 0.2 μM, 0.5 μM and 1 μM) produced HCR products with different length (2000bp, 1000bp, 600bp, 500bp). Longer HCR products meant that more multi-branched arms and more fluorophores could be produced, here 0.1 μM of initiators was used for the subsequent experiments.

3.2. Synthesis and affinity binding analysis of Apt-HCR for target cells

The apt-HCR structure we synthesized could not only recognize target cells and amplify fluorescence signal, but also act as robotic grippers to bind with TDFs multivalently for CTCs' capture and release. The aptamer we used was SYL3c, which had been proved to specifically recognize human cancer cells that express EpCAM (epithelial cell adhesion molecule) [44]. In our study, an extra sequence (Table S1) at the 3′ end of SYL3c aptamer which was complementary to the initiator was designed. In order to verify that the apt-HCR structure could recognize the EpCAM-positive cells and amplify the labeled fluorescence signal, probes of Cy3-labeled apt, Cy3-labeled lib and lib-HCR were used for control experiments. The cell lines we employed were the MCF-7 cells with high EpCAM expression and the control cell lines were Hela cells without EpCAM expression. Both cells lines were divided into 5 groups for affinity binding experiments: Cells only, Cells incubated with apt-HCR (cells + apt-HCR), cells incubated with SYL3c aptamer only (Cells + apt), Cells incubated with random DNA sequence (Cells + lib) and Cells incubated with lib-HCR (Cells + lib-HCR). We used flow cytometry to analyze the

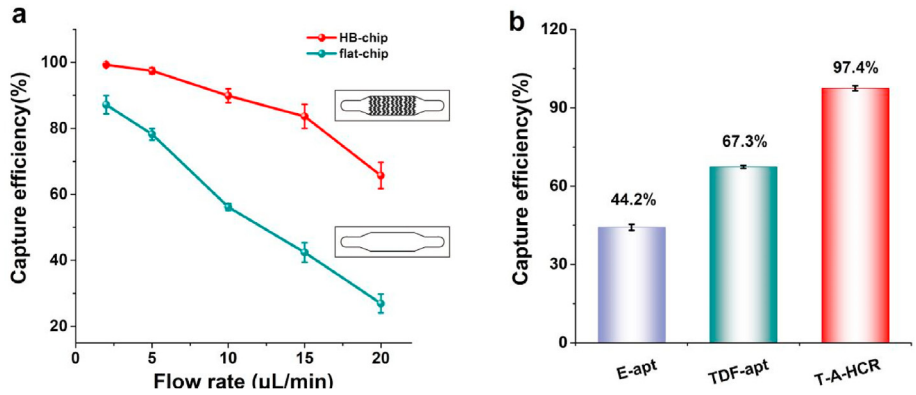

Fig. 3. Comparison of capture efficiency of the T-μFS for 10^5 MCF-7 cells in PBS buffer. (a) by HB-chip and flat-chip at different flow rate conditions. (b) by aptamer alone (E-apt), TDF connect aptamer (TDF-apt) and TDF connect apt-HCR (T-A-HCR) at flow rates of 5 μL/min. Error bars represented standard deviations (n = 3).

affinity binding behavior of capture probes for target cells. As shown in Fig. 2a, for the MCF-7 cell lines experiment, compared with Cells only group, the groups of Cells + lib and Cells + lib-HCR had no fluorescence signal, while the groups of Cells + apt-HCR and Cells + apt had a noticeable fluorescence signal enhancement. As shown in Fig. 2b, for the Hela cell lines experiment, all the cell groups had no fluorescent signal. These results demonstrated that both the aptamer and the apt-HCR structure we designed could recognize the MCF-7 cells well. What is more, fluorescence signal produced by the cells + apt-HCR group was about 5 times higher than that of cells + apt group, proving that the apt-HCR structure had stronger signal amplification ability which was produced by long HCR products with multiple fluorophores (Fig. 2a).

To calculate the binding affinity ability, K_d value of apt/I with MCF-7 cells was calculated. As shown in Fig. 2c, the fluorescence signal increased gradually with the concentrations of apt/I ascending and kept stable when the concentration was higher than 0.1 μM. The K_d value we measured was 4.47 ± 0.53 nM, which was similar to the original SYL3C aptamer report [44]. As longer HCR products could produce more multi-branched arms and more fluorophores, here, 0.1 μM apt/I was chosen to form apt-HCR for the subsequent experiments. The binding ability of apt-HCR to MCF-7 cells was also investigated under fluorescence microscope. Fig. 2d showed that Cy3 modified apt-HCR probes could recognize and bind target MCF-7 cells well. The results of hybridization between TDF and apt-HCR were characterized by electrophoresis. As shown in Fig. S2, the average molecular weight of apt-HCR and TDFs combination product was heavier than that of apt-HCR product only, which proved the hybridization of TDFs with apt-HCR thus achieving multivalent binding.

3.3. Fabrication of microfluidic chip

The purpose of microfluidic chip in the device system was for TDF fixation and CTC capture. We fabricated the microfluidic chip by transparent PDMS cover and glass substrate which was conductive to fluorescence imaging of CTCs. The PDMS layer of the microfluidic chip we fabricated employed herringbone structure (HB-chip) which were staggered periodically, with each mixing cycle defined by two sequential regions of ten chevrons shifted asymmetrically (Fig. S3). The staggered herringbone-induced microvortices could disrupt the laminar flow streamlines that cells travel, causing them to "shift" which could

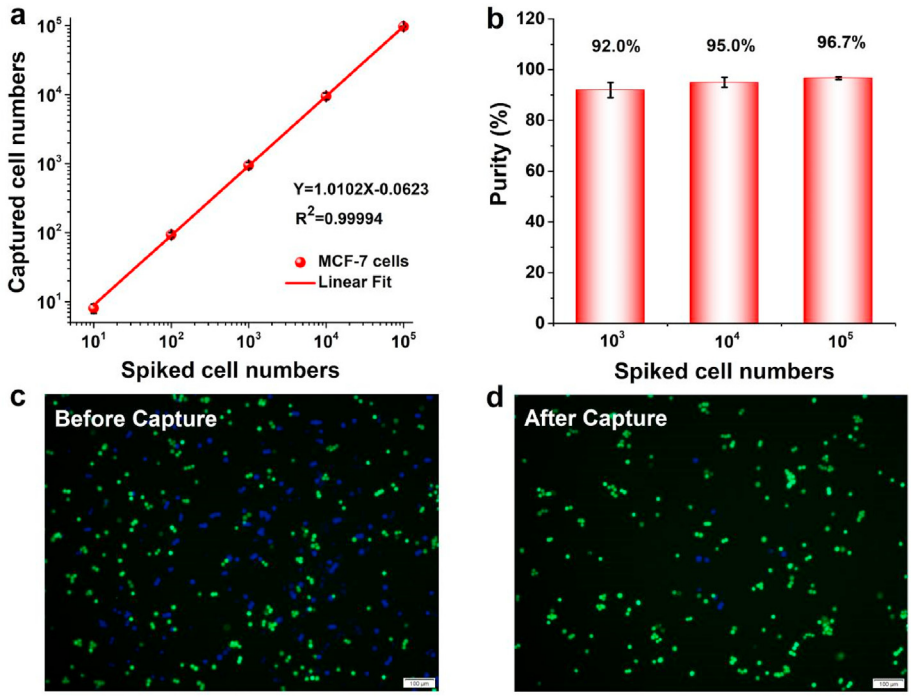

Fig. 4. Capture efficiency and purity of MCF-7 cells in PBS buffer. (a) Regression analysis of the cell number of the MCF-7 cells captured versus the MCF-7 cells spiked in 200 μL of PBS buffer. (b) Capture purity of MCF-7 cells acquired when the cell mixture with cell numbers of both MCF-7 cells and Hela cells were 10^3, 10^4, 10^5 in 200 μL of PBS buffer. Error bars represent standard deviations (n = 3). (c) Representative fluorescence microscope image of the cell mixture containing 10^5 MCF-7 (green) and 10^5 control Hela (blue) before capture. (d) Representative fluorescence microscope image of the cell mixture containing MCF-7 cells (green) and 10^5 control Hela cells(blue) after capture. Scale bar = 100 μm. (For interpretation of the references to color in this figure legend, the reader is referred to the Web version of this article.)

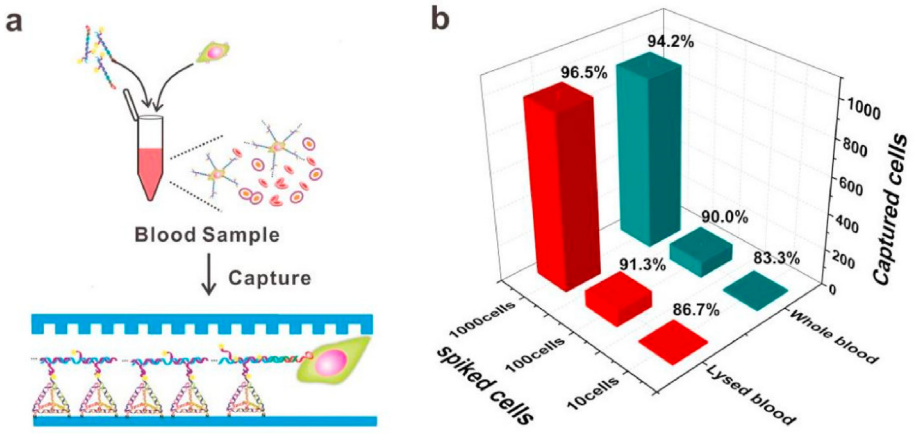

Fig. 5. Capture efficiency of MCF-7 cells in mimic blood samples. (a) Scheme illustration of capture of MCF-7 cells in mimic blood sample. (b) Capture efficiency of MCF-7 cells spiked in 200 μL of lysed blood and whole blood, respectively. Error bars represented standard deviations (n = 3).

significantly enhance the cell surface interactions, leading to higher capture efficiency [17,18]. In recent years, some researchers used Au–S bond to fix the DNA tetrahedral framework on the solid substrate [34,45,46]. However, the high cost of gold substrate and the complicated modification process become the hurdle for practical use [40]. Moreover, as the superquencher, gold could quench fluorophores [47]. Transparent glass substrate with low-cost and commercially available was easily bonded with polymer materials such as PDMS. What is more, amino-modified TDFs can easily be fixed on aldehyde-modified glass substrate by the covalent coupling of amine and aldehyde groups.

3.4. Study on capture performance of the T-μFS in PBS buffer

The T-μFS was set up by connecting a micro syringe pump with a 1 mL syringe to the outlet of the chip via PTFE catheter. The PTFE catheter was used to transfer the liquid solutions. The syringe pump could be adjusted to control the flow rate of solution. The fluorescence microscope was used to observe the stained cells.

To test the effectiveness of HB-chip and optimize the flow rate of the T-μFS, we compared the capture efficiency of MCF-7 cells by the HB-chip and the flat-chip with different flow rate using the T-μFS. As shown in Fig. 3a, the capture efficiency of HB-chip and flat-chip for 10^5 MCF-7 cells were 99.2% and 87.1% separately at the flow rate of 2 μL/min. When the flow rate increased, the capture efficiency of flat-chip decreased much quicker than that of HB-chip. These results showed that HB-chip had higher capture efficiency than flat-chip. At the flow rate of 5 μL/min, the capture efficiency of HB-chip and flat-chip were 97.4% and 78.2% respectively. Here, we chose 5 μL/min as the optimal flow rate for the follow-up experiments. To test the effectiveness of T-A-HCR for capture CTCs using the T-μFS, we compared the capture efficiency of MCF-7 cells by E-apt, TDF-apt and T-A-HCR in the T-μFS. As shown in Fig. 3b, at the flow rate of 5 μL/min, the cell capture efficiency of T-A-HCR for10^5 MCF-7 cells was 97.4%, while the capture efficiency of E-apt and TDF-apt were 44.2% and 67.3% respectively which were much lower than that of T-A-HCR. The reason was that the orientation of the single-stranded probe on the microfluidic interface was uncontrollable, and the probes were prone to entanglement, resulting in the subsequent modification of aptamers with a lower ordered orientation [34,48]. While, the rigid TDFs were highly ordered on the microfluidic interface which not only could segregate neighboring probes avoiding molecular entanglements, but also could place the probes in a solution-phase-like setting to minimize surface steric effects.

In order to verify the capture performance under the optimized conditions determined above, a linear relationship between spiked MCF-7 with different cell numbers (10-10^5) and captured MCF-7 cells in PBS buffer was acquired (Fig. 4a). The linear regression equation was expressed as Y = 1.0102X-0.0623 (R2 = 0.99994). Under different numbers of MCF-7 cells (10 to 10^5), the capture efficiency of our T-μFS was 80.0%, 93.2%, 94.8%, 95.2% and 97.4%, respectively. It was worth mentioning that even when we used 10 MCF-7 cells, which was lower than the minimum cell numbers used in other studies [10,25,49], our T-μFS still had a pretty good capture efficiency. The capture purity for target MCF-7 in PBS buffer by our T-μFS was shown in Fig. 4b. Each of the cell mixtures we used contained both MCF-7 and Hela with the same quantity. The capture purity of MCF-7 cells acquired was 92.0%, 95.1%, 96.7% when the cell numbers of both MCF-7 cells and Hela cells in the cell mixture were 10^3, 10^4, 10^5. Typical images of the cell mixture containing 10^5 MCF-7 and 10^5 Hela were shown in Fig. 4c and d the numbers of MCF-7 cells and Hela cells were basically the same before capture (Fig. 4c), but the MCF-7 cell's number was significantly more than Hela cell's number after captured (Fig. 4d), proving that our T-μFS could capture the target MCF-7 cells specifically.

3.5. Study on clinical utility of the T-μFS using mimic blood samples

To study the clinical practical value of our T-μFS, we applied the optimal conditions to study the capture performance of MCF-7 cells using mimic blood samples (Fig. 5a). As shown in Fig. 5b, the capture efficiency of MCF-7 cells in the lysed blood and whole blood were 86.7%, 91.3%, 96.5% and 83.3%, 90.0%, 94.2% when the numbers of MCF-7 cells range from 10 to 10^3. There is almost no difference for the capture efficiency of MCF-7 cells between the lysed blood and the whole blood, indicating that the capture performance of our T-μFS was not affected by complex blood components and has fairly well clinical applicability. The typical images of captured MCF-7 cells (from 10^3 apt-HCR/MCF-7 cells complex in whole blood) using T-μFS was observed by fluorescence microscope. As seen in Fig. S4, Cy3-labeled apt-HCR probe (red) was both bound well to the surface of the MCF-7 cells (green) and the TDFs on the glass substrate, proving that MCF-7 cells (10^3) in the whole blood were captured in our T-μFS.

3.6. Release and reculture analysis

In order to confirm that our T-μFS not only had good capture performance but also had high release efficiency, release and reculture studies in PBS buffer were conducted using the T-μFS.

Here, nuclease digestion together with high flow rate flushing method was explored for the release of the captured cells (Fig. 6a). We employed benzonase nuclease to digest the captured cells. Compared with protease digestion which was one of the most common method for CTCs' release [31], benzonase nuclease digestion would not destroy cell membrane surface proteins and has little effect on cells' viability. As

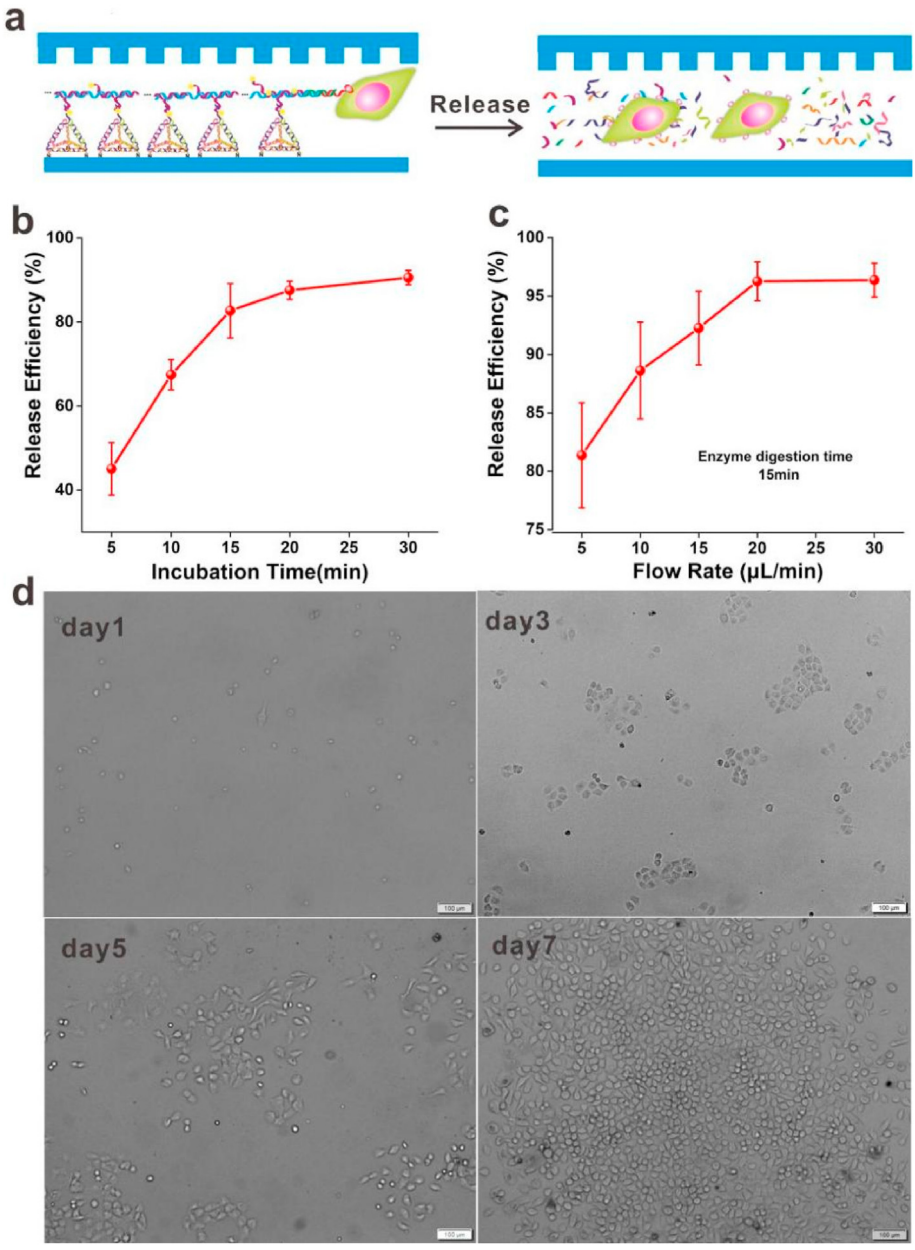

Fig. 6. Release and reculture of MCF-7 cells in PBS buffer. (a) Scheme illustration of CTCs' release. (b) Enzyme incubation time-dependent release efficiency for MCF-7 cells. (c) Rinsing flow rate-dependent release efficiency for MCF-7 cells. (d) Reculture process of the released cells (1, 3, 5, 7days). Scale bar = 100 μm. Error bars represented standard deviations (n = 3).

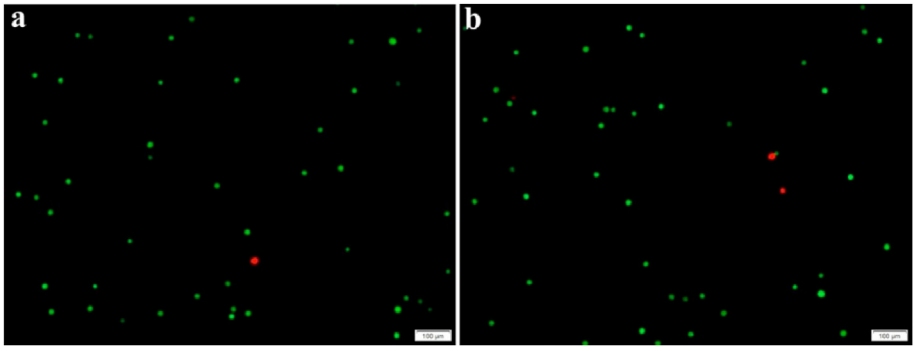

Fig. 7. Fluorescence microscope images of MCF-7 cells (10^3) stained by Calcein-AM/EthD-I. (a) Before being captured and (b) after being released. Scale bar = 100 μm.

Table 1
Comparison of our T-μFS with other technologies and products for capture and release of CTCs.

Methods	Test Sample	Capture Efficiency (%)	Purity (%)	Release Efficiency (%)	Viability (%)	Ref.
Cell Search System	Spiked in whole blood: SKBR-3 cells	85	/	/	/	[24]
Geometrically enhanced mixing system (GEM-chip)	Spiked in PBS: L3.6pl cells	>90	>84	>60	>85	[25]
DNA Nanospheres based microfluidic device	Spiked in PBS: CEM cells	92 ± 4	>80	/	/	[10]
Graphene oxide based microfluidic device	Spiked in PBS: MCF-7 cells	88.2	/	92	/	[50]
TDNs-based microfluidic system (ApTDN-Chip)	Spiked in PBS: SW480 cells	87.4	/	82.4	90.8	[51]
T-μFS in this work	Spiked in PBS: MCF-7 cells	97.4	96.7	96.2	94.6	
	Spiked in whole blood: MCF-7 cells	94.2				

shown in Fig. 6b, with the increase of benzonase nuclease incubation time, the release efficiency of the captured MCF-7 cells increased gradually. When the incubation time reached 15 min, 82.7% of captured MCF-7 cells were released. To improve CTCs' release efficiency, nuclease enzyme digestion together with appropriate high-speed rinsing method was investigated using our T-μFS. As shown in Fig. 6c, for the captured MCF-7 cells incubated with enzonase nuclease for 15 min, the corresponding release efficiency was 81.4%, 88.6%, 92.3%, 96.2%, 96.4% respectively at rinsing flow rate of 5 μL/min, 10 μL/min, 15 μL/min, 20 μL/min and 30 μL/min. Here, 15 min' nuclease incubation time and 20 μL/min rinsing flow rate were chosen as the optimal condition for the release of the captured cells. To prove that the capture and the release treatment by our T-μFS would not affect the MCF-7 cells' viability, Calcein-AM/EthD-1 staining assay was used to evaluate the MCF-7 cells' viability before being captured and after release. Fluorescence microscope images of MCF-7 cells (103) stained by Calcein-AM/EthD-1 were shown in Fig. 7. The MCF-7 cells' viability were 97.5% and 94.6% respectively which meant that there was almost no damage by the capture and release treatment. Furtherly, we conducted the reculture study for the released MCF-7 cells. The released MCF-7 cells were seeded into cell culture dish for propagation. As shown in Fig. 6d, the recultured cells adhered and proliferated well in the culture dish. After 3 days, small cell clusters formed in the dish and grew rapidly, the dish was fully covered with cells after 7 days. The results proved that cells could retain high viability after the capture and release treatment. CK19 and EGFR were validated biomarker for MCF-7 cells. The results of the RT-qPCR showed that the MCF-7 cells cultured could specifically express tumor-specific mRNAs of CK19 and EGFR (Fig. S5) which also proved that the capture and the release treatment by our T-μFS would not damage the MCF-7 cells and could keep the cells viable.

At present, more and more technologies and commercial products have been developed for capture and release of CTCs [10,17,24,25,50,51]. In terms of the capture and release performance, these methods are far from perfect. Our T-μFS showed great capture efficiency, capture purity and release efficiency for simulated CTCs (Table 1), which have a wide application prospect for tumor liquid biopsy.

4. Conclusions

We developed an efficient capture and release system (T-μFS) based on designer tetrahedral framework for multivalent capture and release of CTCs. We first synthesized the TDFs and HCR structures, verified the high affinity of long apt-HCR products to target MCF-7 cells, then we fabricated HB-chip by PDMS cover with designed herringbone structure and TDFs modified glass substrate. After the capture effectiveness of HB-chip and T-A-HCR for MCF-7 cells in the T-μFS were proved, the capture performance of the T-μFS under the optimized conditions was determined. The capture efficiency was from 80.0% to 97.4% when the MCF-7 cell numbers were from 10 to 10^5 and the capture purity was from 92.0% to 96.7% when the cell numbers of both MCF-7 cells and Hela cells in the cell mixture were from 10^3 to10^5 using our T-μFS in PBS buffer. The capture efficiency of MCF-7 cells was from 86.7% to 96.5% and from 83.3% to 94.2% respectively when the cell numbers ranged from 10 to10^3 using our T-μFS in the lysed blood and whole blood. The release efficiency of the MCF-7 cells was 96.2% and the MCF-7 cells' viability before being captured and after release were 97.5% and 94.6% respectively for 10^3 MCF-7 cells using our T-μFS in PBS buffer. Compared with the other current methods for CTC isolation and analysis, our T-μFS showed great advantages with high capture efficiency, high capture purity, high release efficiency and high maintaining capability of cells' viability. Combining with microfluidics chip technology, our T-μFS hopefully could capture and release CTCs integrally and automatically. In the next step, we plan to validate the clinical performance of our T-μFS using patients' blood samples and perform single cell analysis for the captured CTCs. Furthermore, we hope we can develop CTCs derived organoid and organ-on-chip based on the CTCs captured by our T-μFS.

Author contributions

Chenguang Wang: Conceptualization, Methodology, Investigation, Visualization, Writing – original draft, Writing – review & editing. **Yi Xu**: Conceptualization, Methodology, Investigation, Visualization, Writing – review & editing. **Shuainan Li**: Data curation. **Yi Zhou**: Writing – review & editing. **Qiuling Qian**: Data curation. **Yifan Liu**: Funding acquisition, Project administration. **Xianqiang Mi**: Conceptualization, Funding acquisition, Project administration, Supervision, Writing – review & editing.

Declaration of competing interest

The authors declare that they have no known competing financial interests or personal relationships that could have appeared to influence the work reported in this paper.

Acknowledgments

This work was supported by the Program of Shanghai Academic/Technology Research Leader, grant number 20XD1404600; Strategic Priority Research Program of the Chinese Academy of Sciences (In vitro diagnostic technology and equipment); Program of Shanghai Municipal Science and Technology Commission, grant numbers 19511107102 and 20511107600; Chinese Academy of Science, grant number KFJ-STS-QYZD-2021-08-002, National Natural Science Foundation of China, grant number 6190031940.

Appendix A. Supplementary data

Supplementary data to this article can be found online at https://doi.org/10.1016/j.mtbio.2022.100346.

References

[1] J. Massague, A.C. Obenauf, Metastatic colonization by circulating tumour cells, Nature 529 (7586) (2016) 298–306.
[2] S. Gkountela, F. Castro-Giner, B.M. Szczerba, M. Vetter, J. Landin, R. Scherrer, I. Krol, M.C. Scheidmann, C. Beisel, C.U. Stirnimann, C. Kurzeder, V. Heinzelmann-

Schwarz, C. Rochlitz, W.P. Weber, N. Aceto, Circulating tumor cell clustering shapes DNA methylation to enable metastasis seeding, Cell 176 (1–2) (2019) 98–112.
[3] V. Plaks, C.D. Koopman, Z. Werb, Circulating tumor cells, Science 341 (6151) (2013) 1186–1188.
[4] B.M. Szczerba, F. Castro-Giner, M. Vetter, I. Krol, S. Gkountela, J. Landin, M.C. Scheidmann, C. Donato, R. Scherrer, J. Singer, C. Beisel, C. Kurzeder, V. Heinzelmann-Schwarz, C. Rochlitz, W.P. Weber, N. Beerenwinkel, N. Aceto, Neutrophils escort circulating tumour cells to enable cell cycle progression, Nature 566 (7745) (2019) 553–557.
[5] K. Pantel, C. Alix-Panabieres, Liquid biopsy and minimal residual disease - latest advances and implications for cure, Nat. Rev. Clin. Oncol. 16 (7) (2019) 409–424.
[6] P. Ding, Z.L. Wang, Z.E. Wu, W.P. Zhu, L.F. Liu, N. Sun, R.J. Pei, Aptamer-based nanostructured interfaces for the detection and release of circulating tumor cells, J. Mater. Chem. B 8 (16) (2020) 3408–3422.
[7] I.S. Batth, A. Mitra, S. Rood, S. Kopetz, D. Menter, S.L. Li, CTC analysis: an update on technological progress, Transl. Res. 212 (2019) 14–25.
[8] Y.M. Li, S.H. Wu, F. Bai, Molecular characterization of circulating tumor cells-from bench to bedside, Semin. Cell Dev. Biol. 75 (2018) 88–97.
[9] H. Safarpour, S. Dehghani, R. Nosrati, N. Zebardast, M. Alibolandi, A. Mokhtarzadeh, M. Ramezani, Optical and electrochemical-based nano-aptasensing approaches for the detection of circulating tumor cells (CTCs), Biosens. Bioelectron. 148 (2020).
[10] W.A. Sheng, T. Chen, W.H. Tan, Z.H. Fan, Multivalent DNA nanospheres for enhanced capture of cancer cells in microfluidic devices, ACS Nano 7 (8) (2013) 7067–7076.
[11] Y.L. Chen, D. Tyagi, M.S. Lyu, A.J. Carrier, C. Nganou, B. Youden, W. Wang, S.F. Cui, M. Servos, K. Oakes, S.N. He, X. Zhang, Regenerative NanoOctopus based on multivalent-aptamer-functionalized magnetic microparticles for effective cell capture in whole blood, Anal. Chem. 91 (6) (2019) 4017–4022.
[12] F. Odeh, H. Nsairat, W. Alshaer, M.A. Ismail, E. Esawi, B. Qaqish, A. Al Bawab, S.I. Ismail, Aptamers chemistry: chemical modifications and conjugation strategies, Molecules 25 (1) (2020).
[13] S. Bi, S.Z. Yue, S.S. Zhang, Hybridization chain reaction: a versatile molecular tool for biosensing, bioimaging, and biomedicine, Chem. Soc. Rev. 46 (14) (2017) 4281–4298.
[14] D.K. Ye, M. Li, T.T. Zhai, P. Song, L. Song, H. Wang, X.H. Mao, F. Wang, X.L. Zhang, Z.L. Ge, J.Y. Shi, L.H. Wang, C.H. Fan, Q. Li, X.L. Zuo, Encapsulation and release of living tumor cells using hydrogels with the hybridization chain reaction, Nat. Protoc. 15 (7) (2020) 2163–2185.
[15] B.Y. Yuan, L.Y. Guo, K. Yin, X.Y. Wang, Q. Liu, M.M. He, K.D. Liu, J.M. Zhao, Highly sensitive and specific detection of tumor cells based on a split aptamer-triggered dual hybridization chain reaction, Analyst 145 (7) (2020) 2676–2681.
[16] Y.X. Sun, T.A. Haglund, A.J. Rogers, A.F. Ghanim, P. Sethu, Review: microfluidics technologies for blood-based cancer liquid biopsies, Anal. Chim. Acta 1012 (2018) 10–29.
[17] S.L. Stott, C.H. Hsu, D.I. Tsukrov, M. Yu, D.T. Miyamoto, B.A. Waltman, S.M. Rothenberg, A.M. Shah, M.E. Smas, G.K. Korir, F.P. Floyd, A.J. Gilman, J.B. Lord, D. Winokur, S. Springer, D. Irimia, S. Nagrath, L.V. Sequist, R.J. Lee, K.J. Isselbacher, S. Maheswaran, D.A. Haber, M. Toner, Isolation of circulating tumor cells using a microvortex-generating herringbone-chip, P Natl Acad Sci USA 107 (43) (2010) 18392–18397.
[18] A.D. Stroock, S.K.W. Dertinger, A. Ajdari, I. Mezic, H.A. Stone, G.M. Whitesides, Chaotic mixer for microchannels, Science 295 (5555) (2002) 647–651.
[19] J.T. Dong, Y.J. Jan, J. Cheng, R.Y. Zhang, M. Meng, M. Smalley, P.J. Chen, X.H. Tang, P. Tseng, L.R. Bao, T.Y. Huang, D.J. Zhou, Y.P. Liu, X.S. Chai, H. Zhang, A.Q. Zhou, V.G. Agopian, E.M. Posadas, J.J. Shyue, S.J. Jonas, P.S. Weiss, M.Y. Li, G.J. Zheng, H.H. Yu, M.P. Zhao, H.R. Tseng, Y.Z. Zhu, Covalent chemistry on nanostructured substrates enables noninvasive quantification of gene rearrangements in circulating tumor cells, Sci. Adv. 5 (7) (2019).
[20] M.H. Park, E. Reategui, W. Li, S.N. Tessier, K.H.K. Wong, A.E. Jensen, V. Thapar, D. Ting, M. Toner, S.L. Stott, P.T. Hammond, Enhanced isolation and release of circulating tumor cells using nanoparticle binding and ligand exchange in a microfluidic chip, J. Am. Chem. Soc. 139 (7) (2017) 2741–2749.
[21] M. Kozminsky, S. Fouladdel, J.S. Chung, Y. Wang, D.C. Smith, A. Alva, E. Azizi, T. Morgan, S. Nagrath, Detection of CTC clusters and a dedifferentiated RNA-expression survival signature in prostate cancer, Adv. Sci. 6 (2) (2019).
[22] J.T. Dong, J.F. Chen, M. Smalley, M.P. Zhao, Z.F. Ke, Y.Z. Zhu, H.R. Tseng, Nanostructured substrates for detection and characterization of circulating rare cells: from materials Research to clinical applications, Adv. Mater. 32 (1) (2020).
[23] W.Y. Qian, Y. Zhang, W.Q. Chen, Capturing cancer: emerging microfluidic technologies for the capture and characterization of circulating tumor cells, Small 11 (32) (2015) 3850–3872.
[24] W.J. Allard, J. Matera, M.C. Miller, M. Repollet, M.C. Connelly, C. Rao, A.G.J. Tibbe, J.W. Uhr, L.W.M.M. Terstappen, Tumor cells circulate in the peripheral blood of all major carcinomas but not in healthy subjects or patients with nonmalignant diseases, Clin. Cancer Res. 10 (20) (2004) 6897–6904.
[25] W.A. Sheng, O.O. Ogunwobi, T. Chen, J.L. Zhang, T.J. George, C. Liu, Z.H. Fan, Capture, release and culture of circulating tumor cells from pancreatic cancer patients using an enhanced mixing chip, Lab Chip 14 (1) (2014) 89–98.
[26] S. Hou, L.B. Zhao, Q.L. Shen, J.H. Yu, C. Ng, X.J. Kong, D.X. Wu, M. Song, X.H. Shi, X.C. Xu, W.H. OuYang, R.X. He, X.Z. Zhao, T. Lee, F.C. Brunicardi, M.A. Garcia, A. Ribas, R.S. Lo, H.R. Tseng, Polymer nanofiber-embedded microchips for detection, isolation, and molecular analysis of single circulating melanoma cells, Angew. Chem., Int. Ed. 52 (12) (2013) 3379–3383.
[27] M. Tang, C.Y. Wen, L.L. Wu, S.L. Hong, J. Hu, C.M. Xu, D.W. Pang, Z.L. Zhang, A chip assisted immunomagnetic separation system for the efficient capture and in situ identification of circulating tumor cells, Lab Chip 16 (7) (2016) 1214–1223.
[28] S. Hou, H.C. Zhao, L.B. Zhao, Q.L. Shen, K.S. Wei, D.Y. Suh, A. Nakao, M.A. Garcia, M. Song, T. Lee, B. Xiong, S.C. Luo, H.R. Tseng, H.H. Yu, Capture and stimulated release of circulating tumor cells on polymer-grafted silicon nanostructures, Adv. Mater. 25 (11) (2013) 1547–1551.
[29] J.A. Martin, J.A. Phillips, P. Parekh, K. Sefah, W.H. Tan, Capturing cancer cells using aptamer-immobilized square capillary channels, Mol. Biosyst. 7 (5) (2011) 1720–1727.
[30] H.L. Liu, Y.Y. Li, K. Sun, J.B. Fan, P.C. Zhang, J.X. Meng, S.T. Wang, L. Jiang, Dual-responsive surfaces modified with phenylboronic acid-containing polymer brush to reversibly capture and release cancer cells, J. Am. Chem. Soc. 135 (20) (2013) 7603–7609.
[31] S.S. Banerjee, A. Jalota-Badhwar, S.D. Satavalekar, S.G. Bhansali, N.D. Aher, R.R. Mascarenhas, D. Paul, S. Sharma, J.J. Khandare, Transferrin-mediated rapid targeting, isolation, and detection of circulating tumor cells by multifunctional magneto-dendritic nanosystem, Adv Healthc Mater 2 (6) (2013) 800–805.
[32] J.Y. Li, C. Qi, Z. Lian, Q.S. Han, X.H. Wang, S.F. Cai, R. Yang, C. Wang, Cell-capture and release platform based on peptide-aptamer-modified nanowires, Acs Appl Mater Inter 8 (4) (2016) 2511–2516.
[33] Q.L. Shen, L. Xu, L.B. Zhao, D.X. Wu, Y.S. Fan, Y.L. Zhou, W.H. OuYang, X.C. Xu, Z. Zhang, M. Song, T. Lee, M.A. Garcia, B. Xiong, S. Hou, H.R. Tseng, X.H. Fang, Specific capture and release of circulating tumor cells using aptamer-modified nanosubstrates, Adv. Mater. 25 (16) (2013) 2368–2373.
[34] Y.L. Wen, H. Pei, Y. Shen, J.J. Xi, M.H. Lin, N. Lu, X.Z. Shen, J. Li, C.H. Fan, DNA Nanostructure-based Interfacial engineering for PCR-free ultrasensitive electrochemical analysis of microRNA (vol 2, pg 267, 2012), Sci Rep-Uk 3 (2013).
[35] R.P. Goodman, I.A.T. Schaap, C.F. Tardin, C.M. Erben, R.M. Berry, C.F. Schmidt, A.J. Turberfield, Rapid chiral assembly of rigid DNA building blocks for molecular nanofabrication, Science 310 (5754) (2005) 1661–1665.
[36] M.H. Lin, J.J. Wang, G.B. Zhou, J.B. Wang, N. Wu, J.X. Lu, J.M. Gao, X.Q. Chen, J.Y. Shi, X.L. Zuo, C.H. Fan, Programmable engineering of a biosensing interface with tetrahedral DNA nanostructures for ultrasensitive DNA detection, Angew. Chem., Int. Ed. 54 (7) (2015) 2151–2155.
[37] M.H. Lin, Y.L. Wen, L.Y. Li, H. Pei, G. Liu, H.Y. Song, X.L. Zuo, C.H. Fan, Q. Huang, Target-responsive, DNA nanostructure-based E-DNA sensor for microRNA analysis, Anal. Chem. 86 (5) (2014) 2285–2288.
[38] X.Q. Chen, G.B. Zhou, P. Song, J.J. Wang, J.M. Gao, J.X. Lu, C.H. Fan, X.L. Zuo, Ultrasensitive electrochemical detection of prostate-specific antigen by using antibodies anchored on a DNA nanostructural scaffold, Anal. Chem. 86 (15) (2014) 7337–7342.
[39] W.W. Qin, L. Chen, Z.R. Wang, Q. Li, C.H. Fan, M.H. Wu, Y.Q. Zhang, Bioinspired DNA nanointerface with anisotropic aptamers for accurate capture of circulating tumor cells, Adv. Sci. 7 (19) (2020).
[40] Z.H. Li, B. Zhao, D.F. Wang, Y.L. Wen, G. Liu, H.Q. Dong, S.P. Song, C.H. Fan, DNA nanostructure-based universal microarray platform for high-efficiency multiplex bioanalysis in biofluids, Acs Appl Mater Inter 6 (20) (2014) 17944–17953.
[41] T.S. Chen, L.J. Ren, X.H. Liu, M.R. Zhou, L.L. Li, J.J. Xu, X.L. Zhu, DNA nanotechnology for cancer diagnosis and therapy, Int. J. Mol. Sci. 19 (6) (2018).
[42] M.H. Lin, P. Song, G.B. Zhou, X.L. Zuo, A. Aldalbahi, X.D. Lou, J.Y. Shi, C.H. Fan, Electrochemical detection of nucleic acids, proteins, small molecules and cells using a DNA-nanostructure-based universal biosensing platform, Nat. Protoc. 11 (7) (2016) 1244–1263.
[43] R.M. Dirks, N.A. Pierce, Triggered amplification by hybridization chain reaction, P Natl Acad Sci USA 101 (43) (2004) 15275–15278.
[44] Y.L. Song, Z. Zhu, Y. An, W.T. Zhang, H.M. Zhang, D. Liu, C.D. Yu, W. Duan, C.J. Yang, Selection of DNA aptamers against epithelial cell adhesion molecule for cancer cell imaging and circulating tumor cell capture, Anal. Chem. 85 (8) (2013) 4141–4149.
[45] R. Schlapak, J. Danzberger, D. Armitage, D. Morgan, A. Ebner, P. Hinterdorfer, P. Pollheimer, H.J. Gruber, F. Schaffler, S. Howorka, Nanoscale DNA tetrahedra improve biomolecular recognition on patterned surfaces, Small 8 (1) (2012) 89–97.
[46] Y. Peng, Y.H. Pan, Y.W. Han, Z.W. Sun, M. Jalalah, M.S. Al-Assiri, F.A. Harraz, J. Yang, G.X. Li, Direct analysis of rare circulating tumor cells in whole blood based on their controlled capture and release on electrode surface, Anal. Chem. 92 (19) (2020) 13478–13484.
[47] E. Dulkeith, A.C. Morteani, T. Niedereichholz, T.A. Klar, J. Feldmann, S.A. Levi, F.C.J.M. van Veggel, D.N. Reinhoudt, M. Moller, D.I. Gittins, Fluorescence

quenching of dye molecules near gold nanoparticles: radiative and nonradiative effects, Phys. Rev. Lett. 89 (20) (2002).
[48] L. Soleymani, Z.C. Fang, B. Lam, X.M. Bin, E. Vasilyeva, A.J. Ross, E.H. Sargent, S.O. Kelley, Hierarchical nanotextured microelectrodes overcome the molecular transport barrier to achieve rapid, direct bacterial detection, ACS Nano 5 (4) (2011) 3360–3366.
[49] S.T. Wang, K. Liu, J.A. Liu, Z.T.F. Yu, X.W. Xu, L.B. Zhao, T. Lee, E.K. Lee, J. Reiss, Y.K. Lee, L.W.K. Chung, J.T. Huang, M. Rettig, D. Seligson, K.N. Duraiswamy, C.K.F. Shen, H.R. Tseng, Highly efficient capture of circulating tumor cells by using nanostructured silicon substrates with integrated chaotic micromixers, Angew. Chem., Int. Ed. 50 (13) (2011) 3084–3088.
[50] H.J. Yoon, A. Shanker, Y. Wang, M. Kozminsky, Q. Jin, N. Palanisamy, M.L. Burness, E. Azizi, D.M. Simeone, M.S. Wicha, J.S. Kim, S. Nagrath, Tunable thermal-sensitive polymer-graphene oxide composite for efficient capture and release of viable circulating tumor cells, Adv. Mater. 28 (24) (2016) 4891–4897.
[51] J.L. Zhang, B.Q. Lin, L.L. Wu, M.J. Huang, X.R. Li, H.M. Zhang, J. Song, W. Wang, G. Zhao, Y.L. Song, C.Y. Yang, DNA nanolithography enables a highly ordered recognition interface in a microfluidic chip for the efficient capture and release of circulating tumor cells, Angew. Chem., Int. Ed. 59 (33) (2020) 14115–14119.